RESEARCH ARTICLE
doi: 10.2306/scienceasia1513-1874.2026.027

ScienceAsia 52 (1): 2026: ID 2026027: **1–9**

Anti-fouling performance and mechanism of a hydrophobic polysiloxane-coated heater for heated tobacco products

Guangchao Liu[a], Xianglin Li[a], Jianghong Qu[a], Hui Zhang[a], Wenliang Zhang[a], Jingwen Zhang[b], Xi Zhou[b], Liping Huang[b], Ting Fei[a,*], Ji-Xuan Liu[b,*]

[a] Shanghai New Tobacco Product Research Institute Co., Ltd., Shanghai 201315 China
[b] Engineering Research Center of Advanced Glasses Manufacturing Technology (Ministry of Education), Donghua University, Shanghai 201620 China

*Corresponding authors, e-mail: feit@sh.tobacco.com.cn, jxliu@dhu.edu.cn

Received 30 Oct 2025, Accepted 4 Mar 2026
Available online 22 Mar 2026

ABSTRACT: This study developed a methyl phenyl polysiloxane (MPS) coating that integrates high-temperature resistance and hydrophobicity to address the challenge of surface contamination on heaters in heated tobacco products (HTPs)-a novel tobacco product class wherein the tobacco is heated to 300–350 °C, causing pyrolysis without combustion. MPS resin was synthesized via hydrolysis-condensation and applied onto the heater surface using dip-coating followed by high-temperature curing. The coating's chemical structure, morphology, thermal stability, and wettability were characterized by Fourier transform infrared spectroscopy, scanning electron microscopy, thermogravimetric analysis, and contact angle measurement. Anti-fouling performance was evaluated by simulating real operating conditions with an automatic smoking machine, combined with macro-image analysis and microscopic observation. Results show the prepared MPS coating possesses a cross-linked Si—O—Si backbone structure, presenting a continuous and dense surface with a water contact angle of 110.84°, indicating typical hydrophobicity. During high-temperature heating, the coating showed no significant decomposition, with a high mass retention rate of 97.23% at 400 °C, demonstrating excellent thermal stability. Anti-fouling tests revealed that after smoking 20 cigarettes, the contaminated area of the coated heater was significantly reduced by 48.8% compared to the uncoated one, with pollutants transitioning from a dense continuous layer to discrete islands at the microscopic level. This study confirms that the MPS coating inhibits pollutant wetting and continuous deposition from the interface origin by reducing surface energy and enhancing hydrophobicity, providing an effective material solution and theoretical support for long-term anti-fouling protection of HTP heaters.

KEYWORDS: heated tobacco products, anti-fouling, polysiloxane resin, hydrophobicity, surface contamination

INTRODUCTION

In recent years, with the ongoing evolution of the global tobacco market and the continuous development of consumer experience demands, there has been growing interest in innovative tobacco products. Against this backdrop, heated tobacco products (HTPs) have rapidly emerged as a distinct product category [1, 2]. HTPs utilize internal heaters to precisely control temperature, heating specially designed cigarettes to 300–350 °C without combustion. This process generates a nicotine-containing aerosol that meets consumers' expectations for experience. Thanks to their unique technological principles and increasing market acceptance, HTPs have gained significant commercial attention and widespread public interest [3, 4].

The heater is one of the core components of HTPs. Current mainstream heaters mainly include alloy heaters, metal-ceramic heaters, platinum heaters, and graphite heaters. Among them, metal-ceramic heaters have become a more mainstream choice due to their excellent high-temperature stability, uniform heat conduction performance, and significant durability [5–8]. However, metal-ceramic heaters face the challenge of surface contamination during actual service. During the dynamic heating-cooling cycles of actual use, tobacco oil vapor condenses and leaving residues on the heater surface. These residues undergo pyrolysis, carbonization, and interact with oxidation products during subsequent heating cycles, gradually forming a dense fouling layer with complex physicochemical properties on the heater surface. This fouling layer acts as a thermal barrier, not only reducing the overall heat transfer efficiency of the heater but, more critically, leading to uneven heat distribution. This uneven heating destabilizes the pyrolysis process of tobacco, causing fluctuations in aerosol release and generating undesirable odors (such as a burnt taste), ultimately severely affecting product performance stability and user experience. Therefore, improving the surface anti-fouling performance of HTP heaters is crucial for ensuring the stability of these products.

Hydrophobic coatings, typically defined as functional coatings with a water contact angle greater than 90°, exhibit notable anti-adhesion properties due to their low surface energy, effectively reducing the adhesion between the substrate and liquid or semi-solid pollutants such as tobacco oil condensates [9, 10]. This characteristic has led to their wide application in self-cleaning, anti-icing, and other fields [11–14]. In the

context of HTP heaters, a high-temperature-resistant hydrophobic coating can, in principle, create an energy barrier against pollutant deposition by suppressing the spreading and wetting of initial condensate droplets, thereby enhancing the heater's anti-fouling capability. Currently, such coatings are often fabricated from low surface energy materials, primarily silicone resins or fluorocarbon resins. Owing to increasing environmental concerns associated with fluorine, the development of high-performance, fluorine-free hydrophobic coatings has become an important research direction [15]. Among the fluorine-free alternatives, silicone resins are considered promising candidate materials due to their low surface energy, excellent high-temperature resistance, and chemical stability. The soft Si—O—Si backbone and the high bond energy of the Si—O bonds enable the formation of a three-dimensional cross-linked network, which provides good thermal stability and mechanical strength [15–17].

However, single-component polysiloxane coatings, which rely mainly on the shielding effect of $-CH_3$ side groups, often exhibit limited hydrophobicity and heat resistance. Therefore, their performance is frequently enhanced by incorporating modifying components, notably by introducing aromatic groups (e.g., benzene rings or fused rings) which improve thermal stability and rigidity [18]. In this regard, silicone resins modified with aromatic groups, such as MPS, represent a particularly attractive class of materials for high-temperature applications. Theoretically, applying such an aromatic-modified silicone hydrophobic coating to an HTP heater is expected to reduce pollutant adhesion and thus improve anti-fouling performance.

Therefore, to develop an effective anti-fouling solution for HTP heaters, this study designed and fabricated a high-temperature-resistant hydrophobic coating based on the aforementioned MPS. The MPS resin was synthesized via hydrolysis-condensation and applied onto the heater surface via a dip-coating process. The chemical structure, morphology, thermal stability, wettability, and, most importantly, the anti-fouling performance of the coated heater were systematically investigated. The corresponding mechanisms were also elucidated to provide theoretical and technical support for the application of such specialized coatings in HTPs.

MATERIALS AND METHODS

Preparation of the high-temperature-resistant hydrophobic coating

MPS resin was synthesized via hydrolysis. All reagents were of analytical grade and sourced from Titan Co., Ltd., Shanghai, China. Methyltrichlorosilane, dimethyldichlorosilane, diphenyldichlorosilane, and phenyltrichlorosilane were sequentially added to a four-necked flask in molar ratios of 2.0:3.5:2.5:4.3, followed by adding xylene solvent (four times the mass of the monomers), and stirring until completely dissolved. Then, the flask was immersed in a 60 °C water bath with stirring. While stirring, a mixture of acetone (twice the total mass of the monomers) and an excess amount of water was added dropwise to the flask over a period of 90 min via a dropping funnel. The stirring was continued for a total reaction time of 2 h to ensure complete hydrolysis, yielding a silanol solution. After hydrolysis, the reaction solution was transferred to a separatory funnel, allowed to stand for layer separation, the lower aqueous layer was discarded, and the upper oily layer was washed with 60 °C distilled water until neutral. The washed hydrolysate was poured into a single-necked flask equipped with a water separator and reflux condenser. 0.005 wt% of the condensation catalyst tetramethylammonium hydroxide was added, and the mixture was stirred and heated to 120 °C for 12 h. After the reaction, the catalyst was removed by washing with water until the washings were neutral. The solvent xylene was removed under reduced pressure at 110 °C, yielding a fluid oily MPS product [19, 20]. The synthesized product was mixed with xylene to prepare a 50 wt% MPS solution as the coating precursor.

A functional coating was applied to the heater surface using the dip-coating method. To ensure strong adhesion between the coating and the substrate, the heater substrate underwent pretreatment. Before coating, the heaters were sequentially cleaned ultrasonically with deionized water and anhydrous ethanol to remove water-soluble impurities and oily contaminants from the surface. The cleaned heaters were then dried in a 60 °C vacuum oven for 2 h to thoroughly remove residual moisture. Subsequently, the clean, dry heaters were immersed in the prepared MPS solution and withdrawn at a constant rate of 30 cm/min to ensure uniform film formation on the surface. Finally, the MPS-coated heaters were dried at 60 °C for 20 min, then heated to 250 °C at a rate of 5 °C/min and held for 30 min to cure the coating.

Sample characterization and anti-fouling performance evaluation

To systematically evaluate the chemical structure, physical properties, and practical anti-fouling capability of the MPS coating, the following characterization and evaluation methods were employed. A Fourier Transform Infrared Spectrometer with Attenuating Total Reflection (ATR-FTIR, Nicolet 8700, Thermo Nicolet, Tokyo, Japan) was employed to analyze the functional groups within the cured coating. Take 2 ∼ 3 mg of powder and press it evenly onto the diamond crystal ATR module for ATR-FTIR analysis, with a scanning range of 4000–600 cm^{-1}. Thermogravimetric Analysis (TGA, STA 449 F3 Jupiter, NETZSCH, Selb, Germany) was used to assess the thermal stability of the coating. Approximately 5 mg of sample was heated from 50 °C to 400 °C at a rate of 20 °C/min under a dry nitrogen

atmosphere with a flow rate of 60 ml/min, recording its thermal decomposition behavior and mass change [21, 22]. To evaluate the coating's stability under repeated thermal cycling and eliminate the influence of residual solvents, a second heating run was conducted on the same sample under identical conditions. A video contact angle analyzer (CA, Sigma 701, Baioulin Technology, Shanghai, China) was used to measure the static water contact angle of the coating via the sessile drop method to characterize its wettability. Testing was performed at room temperature (25 °C) and 45% relative humidity. A 2.5 µl droplet of deionized water was dispensed onto different positions on each sample surface, and the measurement was repeated three times [23, 24]. To further examine the thermal stability of surface wettability, coated and uncoated heaters were subjected to a heat treatment at 350 °C for 30 min in air. After cooling to room temperature, their water contact angles were remeasured using the same procedure. ImageJ software (Version 1.54p, developed by Wayne Rasband at the National Institutes of Health, Bethesda, USA) was used to fit the angle of the captured droplet images, and the final result was the average of three measurements. In order to evaluate the anti-fouling performance of the coating under realistic operating conditions, a comparative test was conducted in an automatic smoking machine (X500E, Shanghai New Tobacco Product Research Institute Co., Ltd., Shanghai, China) using heaters with and without the MPS coating. The experiment was operated under the following parameters: a heater temperature of 350 °C, a puff volume of 55 ml, a puff duration of 2 s, an interval of 30 s, and a total consumption of 20 cigarettes. Following the test, the coating's efficacy in inhibiting pollutant adhesion was comprehensively assessed through macroscopic observation, scanning electron microscopy (SEM, Maia3, Tescan, Czech Republic), and energy dispersive X-ray spectroscopy (EDS, SU8220, Hitachi, Japan).

RESULTS AND DISCUSSION

Structural characteristics of the coating

Fig. 1 shows the FTIR spectrum of the prepared pristine coating on the heater surface. A weak absorption peak was observed at 3622 cm^{-1}, attributed to the O—H stretching vibration, primarily originating from water molecules adsorbed on the coating surface and possibly partially from residual incompletely cross-linked Si—OH groups from the preparation process [25]. The characteristic double peaks for the asymmetric stretching vibration of the Si—O—Si bond appeared in the range of 1000–1100 cm^{-1}, which is a signature signal of siloxane polymers; the two characteristic peaks correspond to Si—O—Si groups in the silsesquioxane-type cross-linked structure and the chain-like structure, respectively [26–28]. According to literature report [29], during the curing of MPS, the decrease in the Si—OH absorption peak and the increase in the Si—O—Si absorption peak are direct evidence of condensation reactions between silane molecules and the formation of a cross-linked network structure. The spectral features in this study are consistent with this pattern, indicating the successful formation of a stable Si—O—Si cross-linked network.

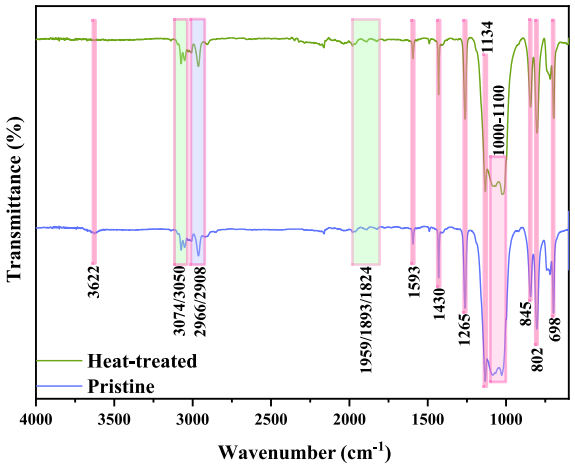

Fig. 1 The FTIR spectrum of the prepared pristine and heat-treated states of prepared coating on the heater surface.

Table 1 Main absorption peaks and their assignments in the IR spectrum of the prepared coating.

Wavenumber (cm^{-1})	Absorption peak type	Ref.
3622	Free —OH vibration	[30]
3074/3050	ν(C—H), —C_6H_5	[31, 32]
2966	ν_{as}(C—H), —CH_3	[33]
2908	ν_s(C—H), —CH_3	[31]
1959/1893/1824/1774	Out-of-plane bending vibration, monosubstituted benzene ring	[34]
1593	Benzene ring in-plane bending vibration	[32]
1430	ν(Si—C), —Si—C_6H_5	[31]
1265	δ(Si—C), —Si—CH_3	[33]
1134	δ(Si—C), —Si—C_6H_5	[31]
1100–1000	ν_{as}(Si—O—Si)	[33]
845	ν(Si—C)	[33]
802	δ(C—H), —Si—CH_3	[33]
698	Benzene ring planar bending vibration, —C_6H_5	[32]

Furthermore, the experimental results were compared and analyzed with the main IR characteristic absorption peaks of methyl phenyl silicone resin reported in the literature (Table 1). Combining Fig. 1 and Table 1, characteristic absorption peaks for methyl, phenyl, and Si—C bonds clearly appear in the spectrum, confirming that methyl and phenyl groups are attached to the silicon atoms as side groups. The introduction of phenyl groups helps enhance the ther-

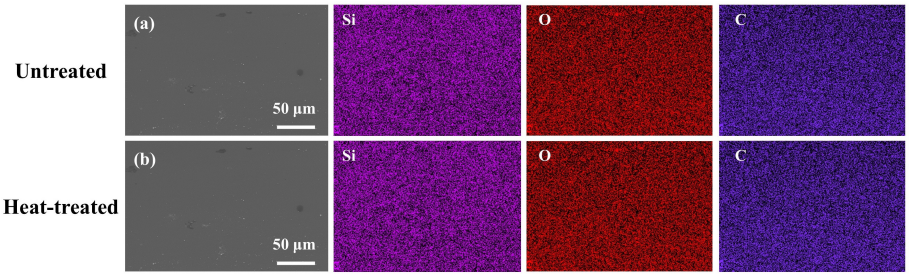

Fig. 2 SEM image and elemental distribution of MPS-coated heater after (a) curing and (b) heat treatment.

mal stability of the polymer, while methyl groups provide low surface energy characteristics, aligning with the goal of this study to develop a high-temperature-resistant hydrophobic coating. Additionally, the coexistence of characteristic peaks for linear and cyclic units in Table 1 indicates that the resin precursor contains these two structural units. Combined with the aforementioned Si—O—Si characteristic peaks as direct evidence of the cross-linked network, it can be concluded that the prepared silicone coating is a cross-linked polymer with Si—O—Si bonds as the main chain and methyl and phenyl groups as side chains.

Surface morphology of the coating

The microstructure and elemental composition/distribution of MPS-coated heater was characterized using SEM and EDS, respectively, with results shown in Fig. 2a. The coating surface is continuous, smooth, dense, and pore-free, with no obvious cracks or defects. This is attributed to the cross-linked structure formed by methyl and phenyl groups connected to the Si—O—Si backbone in the coating molecules. This structure gives the molecules low polarity and strong hydrophobicity, facilitating uniform spreading and the formation of a continuous, dense film on the heater surface [35]. The EDS elemental mapping of the coating surface clearly shows a uniform distribution of the characteristic elements Si, O, and C. It should be noted that hydrogen (H), present in the methyl and phenyl groups, is not detectable by the EDS technique.

Thermal stability of the coating

The thermal stability of the prepared coating on the heater surface in the range of 50–400 °C under an air atmosphere was tested using TGA, with results shown in Fig. 3. During the initial test, when the heating temperature was between 281–352 °C, the coating showed only a slight mass loss of 1.20%. This mass loss originated from the further condensation of incompletely cross-linked Si—OH groups, generating water molecules that volatilized, corroborating the detection of uncross-linked Si—OH characteristic absorption peaks in the previous FTIR analysis [36]. When the temperature was between 352–383 °C, the coating mass loss was about 0.92 wt%, primarily caused by the

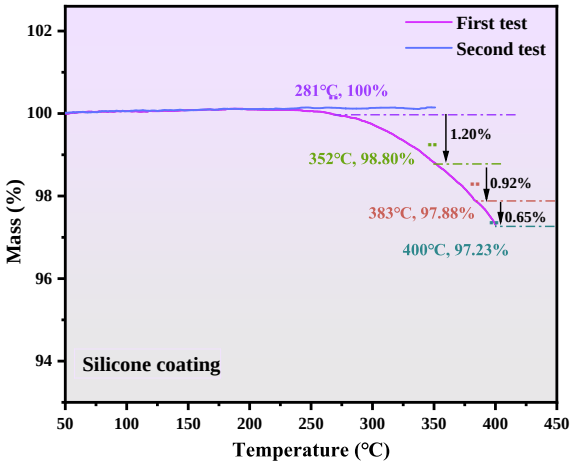

Fig. 3 TGA curve of the prepared coating undergoing cyclic heating in air.

initial condensation of a small number of Si—C bonds and Si—OR groups at this temperature, releasing low molecular weight volatile compounds [37, 38]. When the temperature was between 383–400 °C, the mass loss in this stage was about 0.65 wt%, originating from the depolymerization of some linear siloxane segments releasing cyclic siloxanes and the oxidative cleavage of some Si—C bonds, leading to oxidative decomposition of the coating [37, 38]. Despite this, the coating still maintained 97.23% of its mass at 400 °C. This retention rate is significantly higher than that of similar organic coatings [39, 40], strongly indicating that its main Si—O—Si cross-linked skeleton remains intact at 400 °C. To evaluate the service durability of the MPS coating and eliminate potential interference from residual solvents or thermal history, a second TGA heating cycle was performed on the same sample. The results demonstrate that the coating mass remains constant throughout the ramp-up to the operating temperature (350 °C), with no detectable mass loss observed. This constant-weight behavior during repeated thermal cycling demonstrates that the coating has a good thermal stability.

To verify the thermal stability of the MPS coating

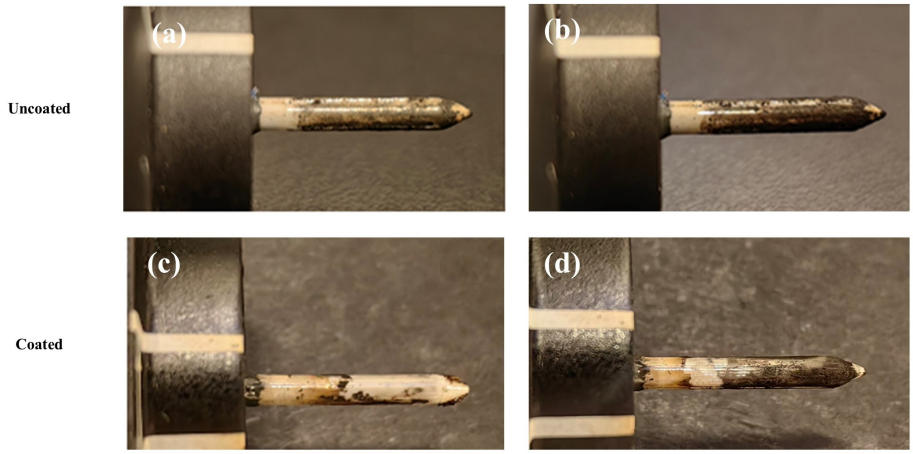

Fig. 4 Macroscopic comparison of heaters after smoking tests: (a) uncoated, 10 cigarettes; (b) uncoated, 20 cigarettes; (c) coated, 10 cigarettes; (d) coated, 20 cigarettes.

at the molecular level, FTIR spectra were recorded after thermal treatment at the operating temperature (350 °C for 30 min), as shown in Fig. 1. The results demonstrate that the characteristic absorption bands of the heat-treated coating are nearly identical to those of the pristine sample. This high degree of spectral consistency indicates that the MPS molecular backbone remains chemically inert without discernible oxidative cleavage or excessive cross-linking under elevated temperatures. Such structural integrity ensures the persistent hydrophobic functionality of the coating from a chemical perspective, enabling stable performance during long-term high-temperature service. SEM and EDS analyses (Fig. 2b) were also employed to assess the physical integrity of the MPS coating after thermal exposure (350 °C for 30 min). The coating retained its smooth and compact morphology without detectable micro-cracks or delamination. The homogeneous elemental mapping further corroborates the chemical stability of the MPS system, indicating its superior resistance to the thermal stresses encountered in heat-not-burn tobacco applications.

In summary, the coating exhibits excellent thermal stability, meeting the high-temperature usage requirements of coating materials for the typical operating temperatures (300–350 °C) of HTP heaters.

Effect of the coating on the anti-fouling performance of the heater

To investigate the practical impact of the MPS coating on the anti-fouling performance of the heater, comparative contamination experiments were conducted on uncoated and MPS-coated heaters by smoking cigarettes. Fig. 4 shows the macroscopic surface morphology of the two types of heaters after smoking 10 and 20 cigarettes, respectively. Visually, the uncoated heater surface (Fig. 4a,b) was covered with a large amount of pollutant, while the MPS-coated heater surface (Fig. 4c,d) showed significantly reduced pollutant adhesion. To further quantify the anti-fouling effect, ImageJ software was used for statistical analysis of the pollutant coverage area. The data show that after smoking 10 cigarettes, the contamination area percentage of the coated heater (10.56%) was relatively reduced by 65% compared to the uncoated heater (30.16%). After smoking 20 cigarettes, the contamination area percentage of the coated heater (30.40%) was relatively reduced by 48.8% compared to the uncoated heater (59.43%). This indicates that the coating exhibits significant anti-fouling advantages at different stages of pollutant accumulation.

Analysis of the pollutants and anti-fouling mechanism

Composition and microscopic morphology of the pollutants

To elucidate the microscopic mechanism of anti-fouling enhancement, characterization of the chemical composition and morphology of the deposited pollutants is essential. Thus, ATR-FTIR analysis was conducted on the residues adhering to the heater surface after smoking tests, with raw tobacco shreds analyzed as a reference (Fig. 5). The spectra of the two samples show substantial overlap, confirming the tobacco-derived origin of the fouling. The broad absorption around 3350 cm^{-1} (O—H stretching vibration) is attributed to water and hydroxyl/phenolic compounds generated from the pyrolysis and dehydration of tobacco components such as glycerol, sugars, and lignin. The peaks near 2920 and 2850 cm^{-1} (aliphatic C—H stretching) correspond to pyrolysis products of waxes, lipids, or cellulose. Spectral features in the region of 1700–1750 cm^{-1} indicate the presence of carbonyl (C=O) groups from aldehydes, ketones, or carboxylic acids formed via pyrolytic oxidation. The peak around 1600–1650 cm^{-1}

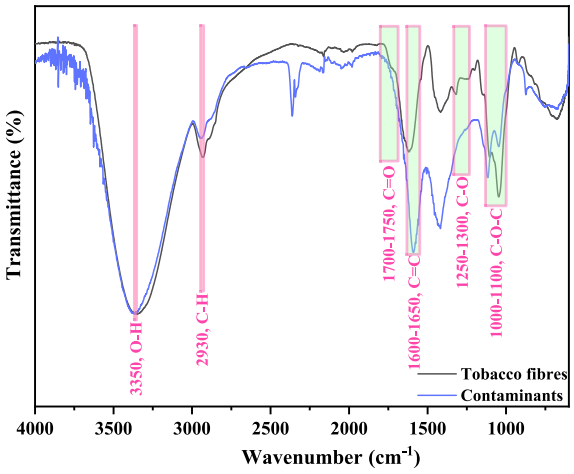

Fig. 5 ATR-FTIR infrared spectra of surface contaminants and tobacco fibres on the heating element after contamination.

(aromatic C=C stretching) reveals aromatic structures, likely including polycyclic aromatic hydrocarbons originating from the pyrolysis of lignin and other aromatic tobacco constituents. Furthermore, absorptions in the ranges of 1250–1300 cm^{-1} and 1000–1100 cm^{-1} are consistent with C—O stretching vibrations from phenols, ethers, and/or sugar degradation products. In summary, the fouling layer primarily consists of a complex mixture of tobacco tar residues resulting from the high-temperature pyrolysis of major tobacco components like sugars, lignin, and lipids, which aligns with previous reports [41, 42].

SEM was further used to characterize the surface microstructure of uncoated and MPS-coated heaters after cumulatively smoking 20 cigarettes. Fig. 6a shows the SEM image of the uncoated heater after smoking. Its surface is covered with a large number of blocky and flaky pollutants, accompanied by protrusions formed by pollutant accumulation. The pollutants present as a continuous, dense thin layer enveloping the heater surface, with obvious microcracks visible locally. In sharp contrast, the MPS-coated heater surface (Fig. 6b) shows a significant reduction in the amount of pollutant. The distribution morphology changes from a continuous film coverage to a discontinuous, discrete island-like distribution, and no obvious cracks are observed on the surface. The difference in these micro-morphologies provides direct evidence for the quantitative results of the macroscopic anti-fouling performance: the significantly reduced contamination area observed macroscopically is microscopically manifested as a morphological transformation of pollutants from "continuous dense coverage" to "discontinuous discrete distribution". This morphological transformation indicates that the MPS coating effectively alters the interaction between the pollutants and the heater surface, inhibiting their ability to spread extensively and form a continuous film. Therefore, combining macro and micro analysis, it can be concluded that the coating primarily enhances the anti-fouling performance of the heater by preventing the continuous and dense deposition of pollutants.

Interfacial wetting mechanism for fouling inhibition

The aforementioned morphological differences indicate that the MPS coating markedly alters the deposition pattern of the pollutants on the heater surface. To reveal the underlying mechanism of the coating's enhancement of heater anti-fouling performance from an interfacial chemistry perspective, this study, combined with the "coating inhibits continuous pollutant deposition" phenomenon observed in the previous SEM characterization, hypothesized that the anti-fouling effect is closely related to the wetting characteristics of the heater surface. To validate this hypothesis, we quantitatively analyzed the surface wettability of the heaters before and after applying the MPS coating through contact angle testing using the sessile drop method, aiming to investigate whether the coating enhances surface hydrophobicity, thereby reducing the tendency for pollutants to wet and adhere, thus elucidating the anti-fouling mechanism from the perspective of interfacial interactions. As shown in Fig. 7, the average contact angle of the uncoated blank heater surface was 37.28° (Fig. 7a), indicating its inherent hydrophilicity and ease of wetting by tobacco oil condensate. After applying and curing the MPS coating, the heater surface contact angle significantly increased to 110.84° (Fig. 7b), exhibiting typical hydrophobic characteristics. This transformation can be attributed to the abundance of non-polar groups in the MPS coating, such as weakly polar alkyl groups (C—H) and hydrophobic structures containing benzene rings. These groups effectively reduce the surface energy of the coating material, thereby imparting good hydrophobic properties [43].

The hydrophobic nature (low surface energy) of the MPS-coated surface, as evidenced by the high water contact angle, plays a decisive role in its anti-fouling performance against the specific pollutants identified in the above Subsection. The tobacco pyrolysis residues are complex mixtures rich in polar functional groups, such as hydroxyls (—OH), carbonyls (C=O), and aromatic rings. According to wetting theory, a low surface energy, non-polar surface (like the MPS coating) exhibits poor wettability by polar substances. This polarity mismatch creates a thermodynamic barrier that impedes the spreading and adhesion of the polar tobacco tar constituents. Consequently, the initial condensates tend to bead up into discrete droplets or islands rather than forming a continuous film, which is consistent with the discrete pollutant morphology observed via SEM (Fig. 6b).

Furthermore, the samples with or without MPS

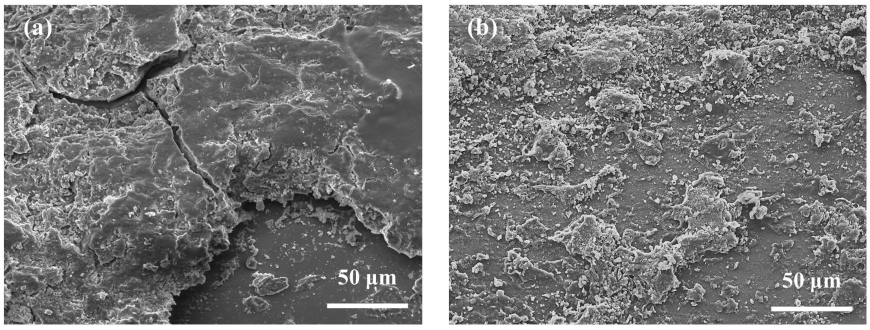

Fig. 6 SEM images of the surface of the heaters after a total of 20 cigarette smoking cycles: (a) uncoated heater; (b) MPS-coated heater.

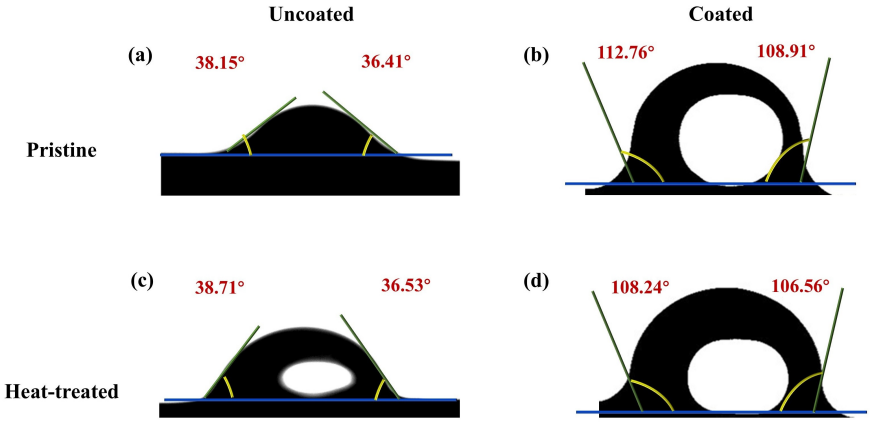

Fig. 7 Water contact angle measurements: (a) uncoated heater surface; (b) MPS-coated heater surface; (c) uncoated heater surface after 350 °C heat treatment; and (d) MPS-coated heater surface after 350 °C heat treatment.

coating were further heated up to 350 °C and dwell at this temperature for 30 min. After cooling to room temperature, their water contact angles were remeasured. As illustrated in Fig. 7, the water contact angles for both the uncoated and MPS-coated heater surfaces remained virtually unchanged before and after the prolonged high-temperature heat treatment, exhibiting no significant hydrophilic shift or functional degradation. This is in agreement with the FTIR, SEM, and TGA results, collectively confirming that the MPS coating maintains a low-surface-energy configuration during extended service.

Combined with SEM analysis, the high-temperature-resistant hydrophobic coating significantly reduces surface energy, weakening the heater's wettability to pollutants, making it difficult for pollutants to spread and form a continuous, dense fouling layer on the surface, ultimately resulting in a significant improvement in anti-fouling performance. The MPS coating significantly enhances anti-fouling performance by reducing surface energy and weakening interfacial wetting toward the pyrolytic tar residues-primarily composed of glycerol, nicotine, and tobacco particles-thereby effectively suppressing pollutant spreading and the formation of dense, continuous fouling layers.

In summary, the improvement in the heater's anti-fouling performance is primarily attributed to the excellent hydrophobicity imparted by the MPS coating. By regulating surface wetting behavior, this coating effectively inhibits the adhesion and deposition of pollutants at the root of interfacial interactions. This study provides a clear mechanistic explanation and experimental support for the anti-fouling application of high-temperature-resistant hydrophobic coatings in HTP heaters.

CONCLUSION

In conclusion, this study successfully developed and systematically characterized a high-temperature-resistant hydrophobic MPS coating to address surface contamination on HTP heaters. The coating forms a stable, cross-linked polymer network featuring Si—O—Si backbones with methyl and phenyl side chains, resulting in a dense, crack-free morphology with excellent thermal stability suitable for HTP operating conditions. Performance evaluations demon-

strated that the MPS coating significantly enhances anti-fouling properties, reducing pollutant adhesion by up to 65% and transforming the contaminant morphology from a continuous dense layer to discrete isolated deposits. This improved performance is mechanistically attributed to a fundamental shift in surface wettability from hydrophilic (37.28°) to hydrophobic (110.84°), driven by the low-surface-energy methyl and phenyl groups. By minimizing the adhesion and spreading of tobacco oil condensate, the hydrophobic surface effectively inhibits the formation of continuous pollutant films, offering a promising strategy for maintaining heater cleanliness and performance in HTP applications.

Acknowledgements: This work was supported by research project of Shanghai New Tobacco Product Research Institute Co., Ltd. (K2023-011Z).

REFERENCES

1. Caputi TL (2017) Industry watch: heat-not-burn tobacco products are about to reach their boiling point. *Tob Control* **26**, 609–610.
2. Baaran R, Güven NM, Eke BC (2019) An overview of iQOS® as a new heat-not-burn tobacco product and its potential effects on human health and the environment. *Turk J Pharm Sci* **16**, 371–374.
3. Liu Y, Cao JX, Zhang J, Chen G, Luo CH, Huang L (2024) Research progress and prospect on the safety of heated tobacco products. *Toxicology* **505**, 153823.
4. Panel EE (2000) A safer cigarette? A comparative study. A consensus report. *Inhal Toxicol* **12**, 1–20.
5. Yang HB, Li YY, Huang YL, Cheng SC, Chen SL, Wang CA, Dong YH (2025) Revisiting 1 GPa alumina ceramics. *J Adv Ceram* **14**, 9221184.
6. Wu ZJ, Wei WX, Yan W, Su YF, Fan HZ, Zhang YS, Song JJ (2025) The influence of solid lubricant addition on the mechanical properties of alumina ceramic materials. *Adv Ceram* **46**, 594–605.
7. Li J, Luo Z, Cui Y, Zhang G, Sun L, Wang J (2024) CMAS corrosion resistance of $Y_3Al_5O_{12}/Al_2O_3$ ceramic coating deposited by atmospheric plasma spraying. *J Inorg Mater* **39**, 671.
8. Huang LY, Wu JT, Zhang JJ, Cao LY, Li JY, Feng LL, Liu YJ, Huang JF (2024) Preparation and photocatalytic activity of oriented cobalt tungstate crystalline glaze. *J Ceram* **45**, 1193–1198.
9. Boinovich LB, Emelyanenko AM (2008) Hydrophobic materials and coatings: principles of design, properties and applications. *Russ Chem Rev* **77**, 583–600.
10. Ahmad D, Van Den Boogaert I, Miller J, Presswell R, Jouhara H (2018) Hydrophilic and hydrophobic materials and their applications. *Energ Source Part A* **40**, 2686–2725.
11. Xu Y, Gao D, Dong Q, Li M, Liu A, Wang X, Wang S, Liu Q (2021) Anticorrosive behavior of epoxy coating modified with hydrophobic nano-silica on phosphatized carbon steel. *Prog Org Coat* **151**, 106051.
12. Meena M, Kerketta A, Tripathi M, Roy P, Jacob J (2022) Moisture barrier layer with supplemental chemical and biological protective functionality for firefighting clothing applications. *J Ind Text* **51**, 6110S–6133S.
13. Choudhary B, Kumar B, Sharma S, Sharma A, Karmakar R, Singh N (2023) Nanotechnology in defence and security. *Emerg Appl Nanomater* **141**, 151–168.
14. Pawar SS, Naik RS, Naik RB, Mahato T, Ratna D (2025) Hydrophobic coatings: An insight into fundamental concepts and modern applications. *Prog Adhes Adhes* **9**, 35–63.
15. Cai G, Wan Y, Liu J, Yang N, Guo J, Li J, Zhou Y, Zhang J, et al (2023) Preparation and performance analysis of methyl-silicone resin-modified epoxy resin-based intumescent flame-retardant thermal insulation coating. *J Micromech Mol Phys* **8**, 61–82.
16. Xiong G, Kang P, Zhang J, Li B, Yang J, Chen G, Zhou Z, Li Q (2019) Improved adhesion, heat resistance, anticorrosion properties of epoxy resins/POSS/methyl phenyl silicone coatings. *Prog Org Coat* **135**, 454–464.
17. Zhang L, Shi Z, Hu W, Zhang X, Zhu H, Zhao G, Wang Z (2018) Curing mechanism, heat resistance, and anti-corrosion properties of a furan/methyl phenyl silicone coating. *Polym Adv Technol* **29**, 1913–1921.
18. Köhler T, Gutacker A, Mejía E (2020) Industrial synthesis of reactive silicones: Reaction mechanisms and processes. *Org Chem Front* **7**, 4108–4120.
19. Gao D, Jia M (2013) Synthesis of poly(methylphenylsiloxane)/phenylene-silica hybrid material with interpenetrating networks and its performance as thermal resistant coating. *J Appl Polym Sci* **128**, 3619–3630.
20. Wang H, Wang J, Wen S, Jiang S, Song J, Ding S, Wu H (2024) Preparation of silicone coating and its anti-ice and anti-corrosion properties. *Coatings* **14**, 699.
21. Zhang GH, Shi JY, Shen HY, Zhang J, Wang JY (2026) Synergistic mechanism of Gd^{3+} and Yb^{3+} on crystallization behavior of CMAS corrosion products. *J Inorg Mater* **41**, 27–36.
22. Zhao CH, Nie GL, Liu YJ, Pang WK, Deng YN, Zuo F, Bao YW (2024) Effects of mixing amount of CoO on non-isothermal crystallization behaviors of willemite crystalline glaze. *J Ceram* **45**, 1245–1254.
23. Tian ZL, Ming KY, Zheng LY, Chen ZL, Zhou F, Liu P, Qiu ZH, Wei DH, et al (2023) *In-situ* observation and mechanism of calcium-magnesium-alumina-silicate (CMAS) melts-induced degradation of RE_2SiO_5 (RE = Tb, Dy, Ho, Y, Er, Tm, and Yb) ceramics at 1500 °C. *J Adv Ceram* **12**, 2315–2330.
24. Li J, Luo ZX, Cui Y, Zhang GH, Sun LC, Wang JY (2024) CMAS corrosion resistance of $Y_3Al_5O_{12}/Al_2O_3$ ceramic coating deposited by atmospheric plasma spraying. *J Inorg Mater* **39**, 671.
25. Zhang J, Guo Y, He L, Huang J, Huang Y, Shang F, Liu R, Zhou X (2025) Study on preparation and fire-resistant property of an organic silicone coating with compounding glass powder. *J Coat Technol Res* **22**, 1087–1097.
26. Shirtcliffe N, Mchale G, Newton M, Perry C (2003) Intrinsically superhydrophobic organosilica sol-gel foams. *Langmuir* **19**, 5626–5631.
27. Dong H, Brennan JD (2006) Controlling the morphology of methylsilsesquioxane monoliths using a two-step processing method. *Chem Mater* **18**, 541–546.
28. Das G, Bettotti P, Ferraioli L, Raj R, Mariotto G, Pavesi L, Sorarù GD (2007) Study of the pyrolysis process of an hybrid $CH_3SiO_{1.5}$ gel into a SiCO glass. *Vib Spectrosc* **45**, 61–68.

29. Batan A, Brusciotti F, De Graeve I, Vereecken J, Wenkin M, Piens M, Pireaux JJ, Reniers F, et al (2010) Comparison between wet deposition and plasma deposition of silane coatings on aluminium. *Prog Org Coat* **69**, 126–132.
30. Fumagalli P, Stixrude L, Poli S, Snyder D (2001) The 10Å phase: A high-pressure expandable sheet silicate stable during subduction of hydrated lithosphere. *Earth Planet Sci Lett* **186**, 125–141.
31. Prado L, Sforça ML, De Oliveira AG, Yoshida IV (2008) Poly(dimethylsiloxane) networks modified with poly(phenylsilsesquioxane)s: Synthesis, structural characterisation and evaluation of the thermal stability and gas permeability. *Eur Polym J* **44**, 3080–3086.
32. Ou DL, Seddon AB (1997) Near-and mid-infrared spectroscopy of sol-gel derived ormosils: vinyl and phenyl silicates. *J Non-Cryst Solids* **210**, 187–203.
33. Mori M, Yoshida IVP (1992) Synthesis and characterization of some poly-*p*-sliphenylenes. *Polym Bull* **29**, 35–42.
34. Young C, Duvall R, Wright N (1951) Characterization of benzene ring substitution by infrared spectra. *Anal Chem* **23**, 709–714.
35. Pan T, Wu H, Guan Z, Zhu X, Hu Y, Fang L, Pei Y, Wu L (2024) OG-POSS synergistically enhances the corrosion resistance and adhesion property of primer for silicone resin thermal protective coating. *React Funct Polym* **205**, 106066.
36. Li JG, Gong GP, Yan CW (2006) Enhancement of the erosion-corrosion resistance of Dacromet with hybrid SiO_2 sol-gel. *Surf Coat Technol* **200**, 4967–4975.
37. Chen X, Zhou S, You B, Wu L (2012) Mechanical properties and thermal stability of ambient-cured thick polysiloxane coatings prepared by a sol-gel process of organoalkoxysilanes. *Prog Org Coat* **74**, 540–548.
38. Bois L, Maquet J, Babonneau F, Mutin H, Bahloul D (1994) Structural characterization of sol-gel derived oxycarbide glasses. 1. Study of the pyrolysis process. *Chem Mater* **6**, 796–802.
39. Gheno G, Ganzerla R, Bortoluzzi M, Paganica R (2015) Determination of degradation kinetics of two polyester thermosetting powder coatings using TGA and colorimetric analysis. *Prog Org Coat* **78**, 239–243.
40. Gao D, Jia M (2012) Thermal degradation, mechanical behavior and Co^{60} gamma-irradiation induced effects of poly(methylphenylsiloxane)/phenylene-silica hybrid material. *High Perform Polym* **24**, 546–558.
41. Polat S, Apaydin-Varol E, Pütün AE (2016) Thermal decomposition behavior of tobacco stem Part I: TGA-FTIR-MS analysis. *Energy Sources Part A* **38**, 3065–3072.
42. Bodnar JA, Morgan WT, Murphy PA, Ogden MW (2012) Mainstream smoke chemistry analysis of samples from the 2009 US cigarette market. *Reg Toxicol Pharmacol* **64**, 35–42.
43. Xu JY, Qi YH, Zhang ZP (2024) Effects of 3,3,3-trifluoropropyl content in poly (dimethyl-methylphenyl-methyltrifluoropropyl) siloxane coating on its antifouling performance. *Prog Org Coat* **197**, 108777.